# STATIC AND DYNAMIC MODEL OF A HTSC AXIAL BEARING

**E. Portabella, R. Palka, H. May and W.-R. Canders**
Institute for Electrical Machines, Traction and Drives
Technical University of Braunschweig
Hans Sommer-Str. 66,
38106 Braunschweig, Germany
R.Palka@tu-bs.de

**ABSTRACT**
The stability of magnetic HTSC bearings under axial perturbations has been experimentally investigated in both quasi-static and dynamic conditions. The obtained results have been then used to develop several numerical models which can reproduce the PM-HTSC behaviour under a wide range of conditions. These calculation methods, implemented in a 2D static finite elements code, have been applied to the design of a rotating bearing for a flywheel energy storage system. The amplitude, frequency and temperature dependence on the stability parameters have been studied and the effects of the obtained results on the bearing performance have been discussed.

## INTRODUCTION

Magnetic bearings enable the relative motion of two machine parts without any mechanical contact and thus, with a minimum of resistance, wear, noise, friction and heat generation. The use of melt-textured high temperature superconductors (HTSC) leads to passive bearing designs where the magnetic forces between the permanent magnets (PM) and the superconducting samples are used to support and stabilise a rotor shaft or a vehicle. The damping is provided by the hysteresis in the magnetisation of the HTSC, so that inherently stable magnetic levitation can be obtained. The absence of a complex feed-back control systems required in the active magnetic bearings opens up the possibility of designing rather simple and compact devices with vanishingly low energy losses. A wide range of potential applications can be found in the field of high speed machines, i.e. turbomachinery or flywheel energy storage systems. Specially promising is also the use of HTSC's in the development of linear bearings for small transport applications operated under clean room and/or vacuum conditions. The conceptual simplicity of HTSC magnetic bearings contrasts with the complex magnetic behaviour of the implied materials. The demagnetising effects associated with the finite dimensions of the samples, the inhomogeneity of the applied field, the hysteretic magnetisation of the superconductor (SC) and its anisotropic current conduction are some of the aspects to be considered when modelling the PM-HTSC force interaction. On the other hand, external perturbations induce a cyclic loading of the bearing which may lead to levitation drift [1] and anomalous dynamics [2]. A full comprehension of the quasi-static and dynamic behaviour of the PM-HTSC arrangement is essential in order to optimise the bearing design and avoid possible instabilities. A static and dynamic model able to contemplate all the previously mentioned phenomena has been developed and validated with experimental measurements. The use of this method as an engineering tool in the design and optimisation of a rotating thrust bearing is presented in this paper.

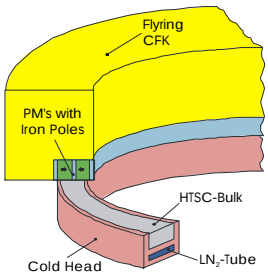


| | **Width** (mm) | **Height** (mm) |
|---|---|---|
| **SC** | 33 | 6 |
| **PM** (×2) | 13.5 | 20 |
| **Fe** (×3) | 3 | 10 |

**FIGURE 1:** Exemplary basic bearing topology with multipolar PM-HTSC arrangement

The exemplary basic bearing configuration (Fig. 1) is composed of a multipolar PM arrangement and several HTSC's. The PM's are embedded in the inner part of a carbon fibre flywheel, disposed in a flux concentrating arrangement. The SC samples are placed in a cold head with an attached cooling tube for the liquid nitrogen ($LN_2$). The rotor has a total weight of 400 kg while the average diameter of the bearing is set to 60 cm. The optimised dimensions [3] are also shown in Fig. 1.

## EXPERIMENTS

In order to study the quasi-static behaviour of the HTSC-PM arrangement and compare the results with the dynamic measurements, a new experimental test bench has been built up (Fig. 2). The system consists of a three co-ordinates table, which can be moved by means of three coupled step-by-step motors. A force sensor fixed to the z-axis is used to measure the axial component of the magnetic force. The superconducting sample is fixed to a fibre glass container mounted on the co-ordinates table.

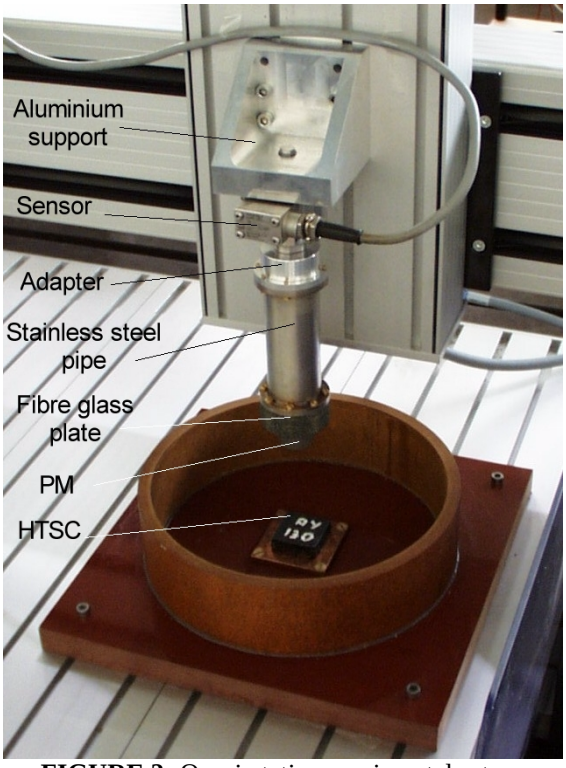


**FIGURE 2:** Quasi-static experimental set up

The system has been used to explore the influence of the activation process on the force and stability parameters as well as the nature of the levitation drift in quasi-static conditions and the force relaxation due to the flux creep effect. The amplitude dependence of the stiffness, *k*, and the hysteresis losses per cycle, $S_n$, is shown in Fig. 3. The minor loops have been applied when the PM was placed at 3.75 mm over the HTSC surface. As can be observed, the magnetic stiffness decreases as the amplitude of vibration increases. That is, for a given equilibrium gap, the recovering elastic force exhibits a degressive characteristic. While for small amplitudes of vibrations the function *k(A)* can be assumed as linear, a more complex dependence should be adopted for higher values of *A*. The non-linearity of *k* increases as the PM-HTSC distance tends to zero. On the other hand, as Fig. 3 exhibits, the hysteresis losses increase with the vibration amplitude following a quadratic function $S_n(A)$.

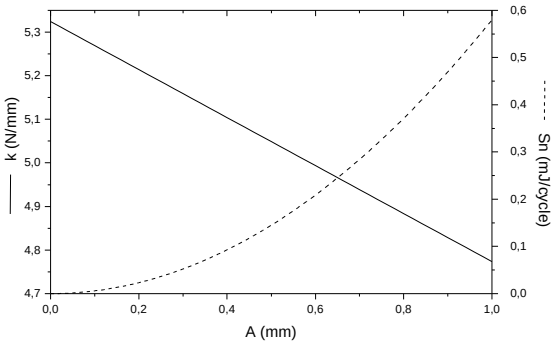


**FIGURE 3:** Amplitude dependence of the stiffness and hysteresis losses per cycle.

The dynamic properties of the PM-HTSC interaction have been investigated using the experimental system shown in Fig. 4. The PM has been coupled to an electromechanical shaker, so that it can be vibrated within a wide range of amplitudes and frequencies. Acceleration sensors have been used to monitor the temporal evolution of the air gap and to control the amplitude of vibration as the system is operated in closed-loop configuration. On the other hand, the HTSC has been placed in a closed cryocontainer directly coupled to a piezoelectric force transducer (Kistler) which enables the measurement of the levitation force. The cryocontainer has been fixed to a very stiff aluminium frame which is directly coupled to the foundation of the shaker. The natural frequencies of the frame have been experimentally and numerically evaluated finding that the first resonant mode lies around 650 Hz, what is far above the measurement range. Finally, to insure that external perturbations will not affect the measured signals, the whole set up has been mounted on air springs, providing a high isolation against the environment. The acquisition, conditioning and representation of the experimental signals are possible thanks to a multianalyser system (Brüel&Kjær), consisting in eight analogue to digital interface modules and a PC where a monitoring application is running.

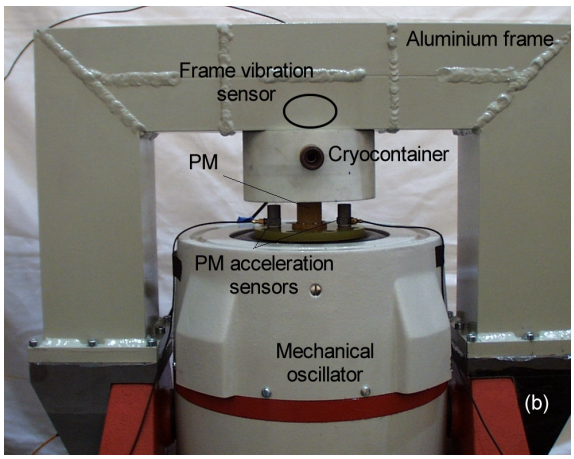


**FIGURE 4:** Set up for dynamic experiments

Using this experimental set up the magnetic behaviour of the PM-HTSC interaction has been explored for vibrations in the frequency range between 10 and 500 Hz and amplitudes between 31.25 µm and 1 mm (Fig. 5). In rotating bearings large amplitude vibrations ($A_{max}$≅1 mm) may be expected while passing the critical frequencies, that is below 200 Hz. On the other hand, much lower frequencies of maximal 20 to 30 Hz and high amplitudes may be likely for linear bearings. Low amplitude and high frequency vibrations can appear in rotating bearings as they are operated at the nominal speed.

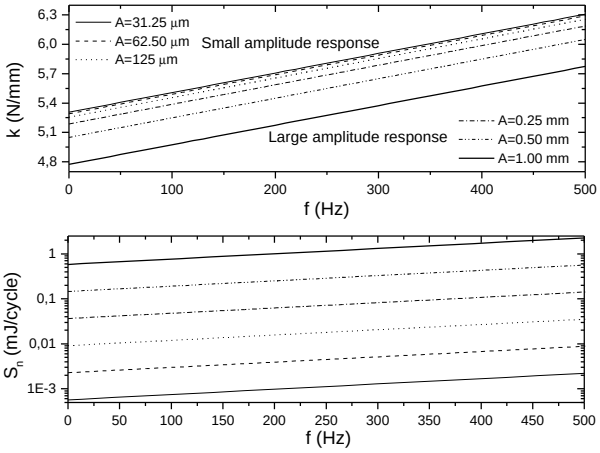


**FIGURE 5:** Frequency dependence of the stiffness and hysteresis losses per cycle.

The weak frequency dependence of the stiffness and damping functions, namely 0.002 N/mm per Hz and 0.032 mJ/cycle per Hz, can be attributed to two different phenomena. First, the presence of flux flow in the HTSC sample which produces an increment of the magnetic damping. Notice that, as the vibration amplitude remains constant and the frequency grows, larger forces are obtained leading to higher values of stiffness and hysteresis losses per cycle. On the other hand, the fast varying magnetic field in the SC produces eddy currents in the surface of the excitation magnet. This effect may be specially important at high frequencies and in PM arrangements including flux collecting iron poles in the proximity of the air gap.

## COMPUTATIONS

### HTSC characterisation: VCJ model

The first step in the design process is to characterise the HTSC samples to be used in the magnetic bearing. Four single-domain pellets (36×36×12 $mm^3$) have been tested in a first approximation. By using a newly developed computational method the critical current density, $J_C(B)$, can be estimated from simple quasi-static force measurements obtained with the experimental set-up shown in Fig. 2. Repulsive forces between 60 and 70 N have been measured with a SmCo cylinder (∅25 mm, h12 mm, iron back pole). The numerical method, called Vector Controlled Jc model (VCJ model), is based on the critical state model of the SC, where bulk currents are induced in the sample to avoid the variation of the magnetic flux inside the material. In the superconducting region two degrees of freedom exist, namely the magnetic flux and the induced current density. An iterative process to obtain the final current density distribution which minimises the changes of the magnetic field within the HTSC has been developed. This method has been successfully applied to reproduce the hysteretic magnetic behaviour of hard SC's using different $J_C(B)$ functions as input [4].

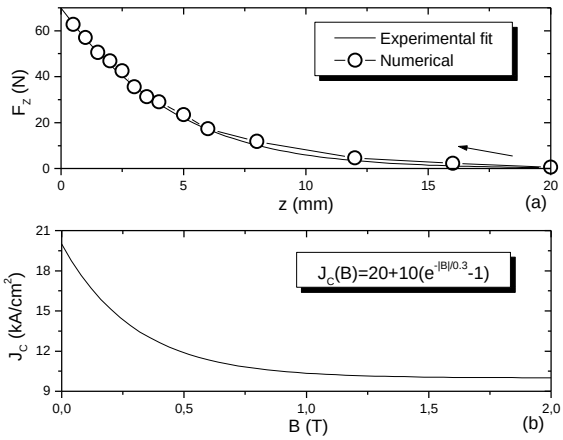


**FIGURE 6:** Force curve (a) and critical current density (b) for the basic PM-HTSC arrangement.

The computed repulsive force is shown in Fig. 6a. As can be observed the average experimental curve can be reproduced with an error under 5% for distances in the range of 0.5 to 8 mm. In this case an exponential $J_C(B)$ dependence has been used, obtaining a maximal value of 20 kA/$cm^2$ at zero applied field (Fig. 6b).

### Support force: VCJ vs. Meissner model

The obtained effective $J_C(B)$ function that characterises our HTSC samples can now be used to evaluate the support force for the optimised PM-HTSC arrangement (Fig. 1). The computed force after an operational field activating process with offset (OFCo) with an initial gap of 13 mm is displayed in Fig. 7a. A maximal force of 8 kN at a distance of 1 mm has been estimated with the VCJ model. Notice that this method produces a considerably more accurate result than that obtained with the simple Meissner approximation, $F_Z$(1 mm)≅16kN, where the SC is considered to react with infinite surface current densities which completely avoid any field change within the sample.

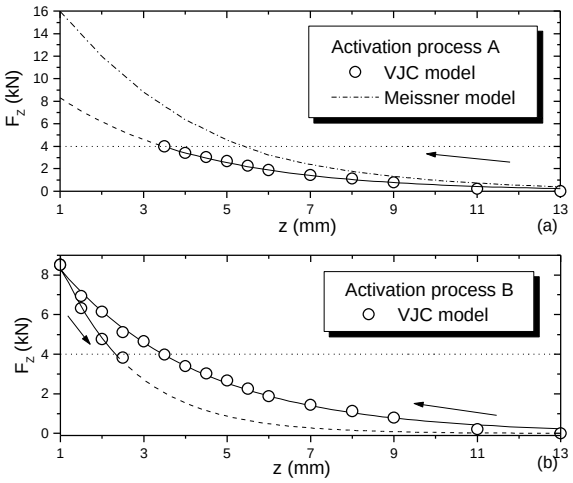


**FIGURE 7:** Computed support forces for the activation processes A and B.

The activation process A consists of lowering the rotor slowly until the total weight is equilibrated by the repulsive PM-HTSC force. An alternative activation process is illustrated in Fig. 7b. In this case the rotor is pressed down reducing the air gap to 1 mm. As the external pressure is released the bearing moves to the nearest equilibrium position, setting the operational gap at approximately 2.5 mm. Due to the increased flux penetration rather higher axial and lateral stiffness values can be obtained with process B.

### Temperature dependence: $J_C(T)$

The influence of the temperature on the support force can be estimated by using different critical current density functions. A logarithmic $J_C(T)$ dependence has been assumed according to the typical data found in the literature [5]. Fig. 8 shows different force curves obtained for temperatures of 77, 60, and 40°K. As can be observed considerably higher forces and stiffness values can be obtained at low temperatures.

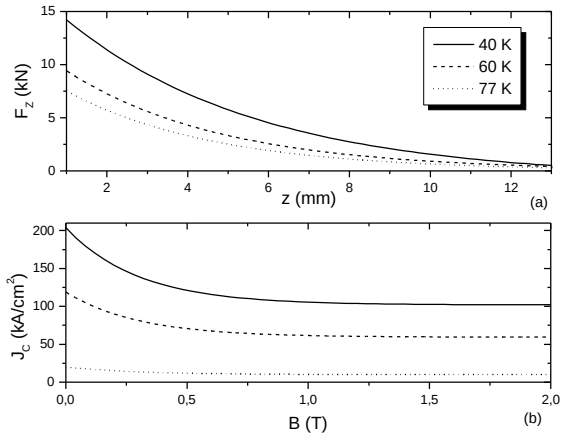


**FIGURE 8:** Computed support forces at different operating temperatures.

### Stiffness matrix: Trapped flux model

The stable levitation of a rigid spinning rotor requires a positive magnetic stiffness for at least five of the six rigid body modes. In the HTSC samples, torques are only developed in reaction to a flux change, that is, for a symmetric applied magnetic field, it may be assumed that the rotation about the symmetry axis is allowed without producing any drag torque. In general, for very small perturbations the restoring force on the PM rotor can be computed by using the trapped flux model where the magnetic vector potential at the HTSC boundaries is computed to maintain the flux distribution inside the material unchanged. Considering the axial symmetry, the stiffness matrix can be written as

$$[k]=\begin{bmatrix} k_r & 0 & 0 & 0 & k_{jr} & 0 \\ 0 & k_r & 0 & -k_{jr} & 0 & 0 \\ 0 & 0 & k_a & 0 & 0 & 0 \\ 0 & -k_{jr} & 0 & k_{jj} & 0 & 0 \\ k_{jr} & 0 & 0 & 0 & k_{jj} & 0 \\ 0 & 0 & 0 & 0 & 0 & 0 \end{bmatrix} \qquad (1)$$

where $k_a=k_{zz}$, $k_r=k_{xx}=k_{yy}$, $k_{jj}=k_{jxjx}=k_{jyjy}$ and $k_{jr}=-k_{jxy}=k_{jyx}$. The obtained values are shown in Tab.1.

**TABLE 1:** Computed stiffness constants

| Stiffness constants | Computed values |
|---|---|
| $\mathbf{k_a}$ (N/m) | 2,272,000 |
| $\mathbf{k_r}$ (N/m) | 1,240,000 |
| $\mathbf{k_{jj}}$ (N/rad) | 2,256,500 |
| $\mathbf{k_{jr}}$ (N/rad) | 298,080 |

### Amplitude dependence: Hybrid model

The amplitude dependence of the axial stiffness and damping constants can be estimated by using an hybrid calculation method, which combines both the VCJ model and the trapped flux model. The first is used to compute the current density distribution in the SC as the activation process takes place. Stiffness and hysteresis losses for large perturbations, $k(A_0)$ and $S_n(A_0)$, can also be estimated with this method (Fig. 9).

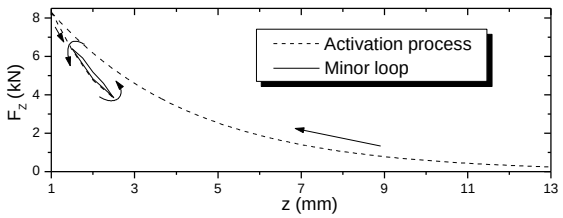


**FIGURE 9:** Large amplitude response.

The system response to vanishingly small disturbances can be reproduced with the trapped flux model, obtaining the stiffness constant k(A≅0). Here, the initial field in the SC is given by a magnetic field generated by the PM and the $J_C$ distribution induced in the SC during the activation process and computed with the VCJ model.

According to our experimental results the amplitude dependence of the stability parameters can then be approximated as

$$k(A) = k(0) - \frac{k(0) - k(A_0)}{A_0} A \qquad (2)$$

and

$$S_n(A) = \frac{S_n(A_0)}{{A_0}^2} A^2 \qquad (3)$$

In the explored case, the following functions have been obtained

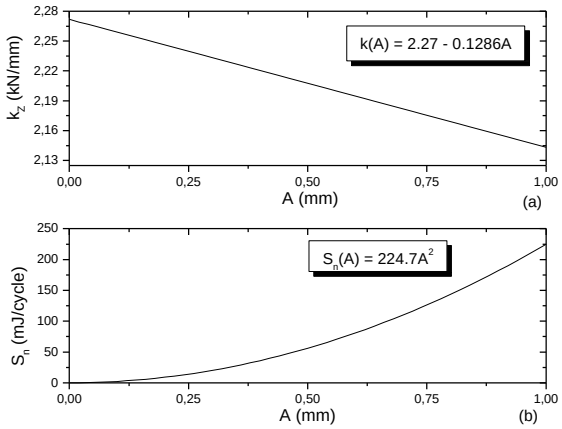


**FIGURE 10:** Amplitude dependent stiffness and hysteresis losses.

**Frequency dependence: Flux flow and creep model**

The VCJ model has been modified in order to include the effects of the flux flow and flux creep phenomena. The flux creep produces a time decay in the magnetic force which may involve the appearance of a drift in the levitation height. On the other hand, the flux flow effect is strongly related with the dynamic behaviour of the PM-HTSC interaction. The contribution of such phenomenon to the increment of the stiffness and the hysteresis losses per cycle has been discussed in the experimental section of this paper.

The FEM code has been modified enabling the calculation of the electric field, *E*, in the SC region. The relation between *E* and the current density in the flux flow and flux creep region is shown in Fig. 11.

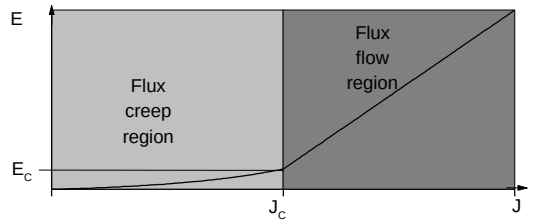


**FIGURE 11:** Electric field vs. current density.

The mathematical expressions of this relation [6,7], which contain terms as pinning potential, flux resistivity and creep resistivity, have been included in the program to correct the computed current distribution in the HTSC. Fig. 12 shows the estimated frequency dependence of the stiffness and the hysteresis losses for the designed bearing and a perturbation amplitude of ±1 mm.

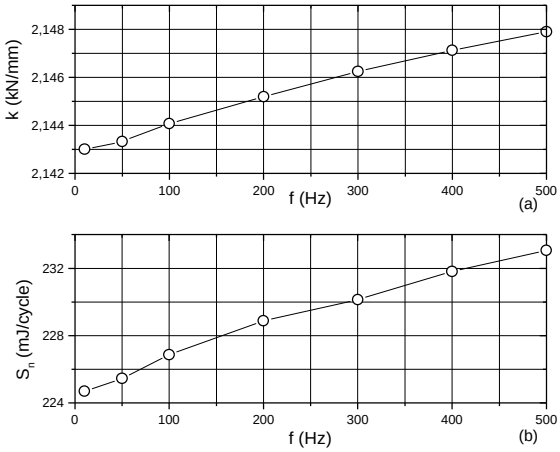


**FIGURE 12:** Frequency dependent stiffness and hysteresis losses.

As can be observed a very weak frequency dependence of the stability parameters exists for this configuration. Notice that in the computations the eddy currents within the excitation system have not been considered.

The flux flow and creep model can also be successfully applied to evaluate the force relaxation effect associated with the flux creep phenomena.

**Dynamic behaviour: Spring-damper model**

Finally, using the obtained functions *k(A,f)* and $S_n(A,f)$ a dynamic model of the PM-HTSC interaction based on the analogy with a spring-damper model has been developed. The axial motion of the levitated flyring can be expressed by a second order non-homogenous differential equation containing non-linear stiffness, *k*, and damping, *h*, terms:

$$k(z,\Omega) = \left(1 + k_f \Omega\right)\left(k_l - k_{nl}|z|\right) \qquad (4)$$

and

$$h(\dot{z},\Omega) = \left(1 + h_f \Omega\right)\left(h_l + h_{nl}|\dot{z}|\right) \qquad (5)$$

For amplitudes of vibration up to 1 mm and frequencies in the range of 10 to 500 Hz, the proposed model has shown to be able of reproducing the behaviour of the PM-HTSC arrangement in terms of stiffness and energy losses with errors under 10%.

The non-linear differential equation has been solved by using the averaging method and the steady state amplitude response *r* has been computed for different values of the external excitation force. Fig. 13 presents two extreme cases, namely static deflections of p=1 mm and p=10 μm, which correspond to external forces of 2.27 kN and 22.7 N. The resonant frequency of the system is about 11.9 Hz for a rotor weight of 400 kg.

In this figure, the region labelled as I encloses the stable vibration states, whereas II indicates unstable or divergent vibrations. Region III is entered when the amplitude response exceeds the levitation gap, that is 2.5 mm. Then a crash between the HTSC and the PM takes place leading the magnetic bearing to collapse. For values of *r* between 1.5 mm and 2.5 mm, the levitation drift phenomenon is observed. These responses are contained in region IV.

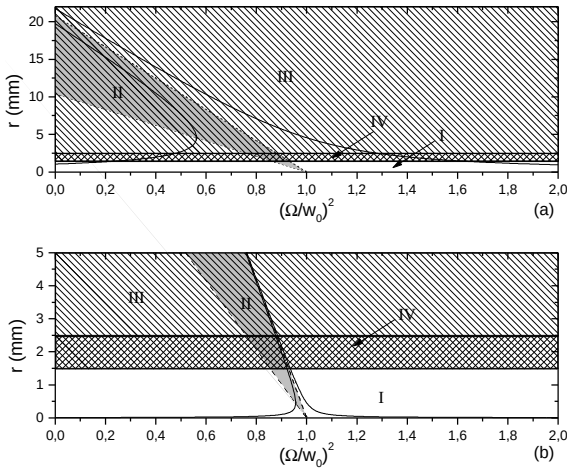


**FIGURE 13:** Amplitude response and instability regions for p=1 mm (a) and p=10 μm (b)

For p=1 mm the drift appears between 6.13 and 8.3 Hz in the increasing frequency branch and between 13.5 and 15.5 Hz in the decreasing one. Any vibration between 8.3 and 13.5 Hz leads to instability and produces the collapse of the bearing. Frequencies outside the regions III and IV, that is 15.5 Hz<f<6.13 Hz, are associated with stable vibrations which ensures a normal operation of the flywheel.

In the second case, p=10 μm, as the vibration frequency is slowly increased the bearing remains stable for any value of *f*. At 11.73 Hz the jump phenomenon appears producing a sudden increment in the amplitude response from 0.49 to approximately 1 mm. If the frequency is decreased the levitation drift appears at 11.6 Hz and the bearing collapses at 11.3 Hz.

Notice that, the unstable states are located far under the operational speeds of the flywheel. For vibration amplitudes up to ±1 mm, the instability region lies between 930 and 967 rpm. Assuming that the system is designed to spin at approximately 10000 rpm, the only way to destabilisation is the oscillation of the unbalanced rotor during the running-up process. Near the resonance vibration amplitudes of approximately 50 μm can be accepted. If the unbalance exceeds this value the bearing should be rapidly accelerated near the resonance avoiding the formation of the steady state response.

## CONCLUSIONS

The static and dynamic properties of a basic PM-HTSC arrangement have been investigated with two newly designed experimental set-ups. For perturbation amplitudes increasing up to 1 mm, a linear decay of the stiffness has been observed. On the other hand, the magnetic damping or hysteresis losses per cycle exhibits a quasi exact quadratic increase with the amplitude of vibration. Both parameters have shown a very weak frequency dependence in the explored range. Such behaviour has been simulated in several numerical calculation methods which have been applied to the design of a rotating bearing. The VCJ model reproduces the HTSC hysteretic behaviour and enables the estimation of an effective critical current density function, where the temperature dependence can be easily included. The trapped flux model enables the computation of the stiffness matrix, while the limitations of the discretisation to reproduce the HTSC response to very small perturbations have been solved with the hybrid model. The time-frequency dependence has been reproduced with the flux flow and creep model. A non-linear spring-damper model has been used to evaluate the dynamic response of the bearing to axial perturbations, identifying the critical frequencies and amplitudes which may lead to instability or levitation drift.

## REFERENCES

1. T.A. Coombs, A.M. Campbell, *Gap decay in superconducting magnetic bearings under influence of vibrations*, Physica C 256 (1996) 298-302.
2. T. Hikiahra, T. Fujinami and F.C. Moon, *Bifurcation and multifractal vibration in dynamics of a high-Tc superconducting levitation system*, Phys. Lett. A 231 (1999) 217-223.
3. W.-R. Canders, S. Siems, H. May, R. Palka and E. Portabella, *Application of high Tc superconducting magnetic bearings for contactless suspension of high speed machines*, Proc. of the ISMB 2000, Zurich (Switzerland), (to be presented)
4. R. Palka, E. Portabella, H. May and W.-R. Canders, *Axis-symmetric finite element analysis of the permanent magnet-superconductor interaction*, Proceedings of the ISTET 1999, Magdeburg (Germany).
5. M. Murakami, *Melt processed high-temperature superconductors*, World Scientific (1992)
6. P.W. Anderson, *Theory of flux creep in hard superconductors*, Phys. Rev. Lett. 9 (1962) 309-311.
7. Y.B. Kim, C.F. Hempstead and A.R. Strand, *Flux-flow resistance in type-II superconductors*, Phys. Rev. 139 (1965) 1163-1172

## ACKNOWLEDGEMENTS

This work has been supported by the European Commission under contract No. ERBFMBICT 983507 and the German BMBF under contract No. 13N6658/2.